**Aalborg Universitet**

# Flexible Control Strategy for Grid-Connected Inverter under Unbalanced Grid Faults without PLL

Guo, Xiaoqiang; Liu, W.; Zhang, X.; Sun, X.; Lu, Z.; Guerrero, Josep M.

[Link to publication from Aalborg University](#)

# Flexible Control Strategy for Grid-Connected Inverter under Unbalanced Grid Faults without PLL

Xiaoqiang Guo, *Member, IEEE*, Wenzhao Liu, Xue Zhang, Xiaofeng Sun,
Zhigang Lu and Josep M. Guerrero, *Senior Member, IEEE*

*Abstract*—**Power oscillation and current quality are the important performance targets for the grid-connected inverter under unbalanced grid faults. Firstly, the inherent reason for the current harmonic and power oscillation of the inverter is discussed with a quantitative analysis. Secondly, a new control strategy is proposed to achieve the coordinate control of power and current quality without the need for a phase-locked loop (PLL) or voltage/current positive/negative sequence extraction calculation. Finally, the experimental tests are conducted under unbalanced grid faults, and the results verify the effectiveness of the propose method.**

*Index Terms*—**grid-connected inverter, grid fault, weak grid, current quality, power oscillation, PLL**

## I. INTRODUCTION

Power-electronic-interfaced renewable energy systems (RES) receive more and more attention around the world. In order to achieve the flexible operation of RES, many technical challenges should be dealt with, and one of the most important issues is how to ride though the short-term disturbances, especially under unbalanced grid faults.

Many interesting solutions have been presented in the past few years, and they can be divided into two categories, one is the rotating-frame solution, and the other is the stationary-frame solution. A dual-sequence rotating frame control was reported in [1], which achieves the constant dc voltage without active power oscillations. An enhanced dual-frame control was presented in [2]. The dynamic response is improved by using the decoupling network. Another interesting method was proposed in [3]. The multiple-rotating-frame control was used to mitigate the effect of grid background harmonics. The major disadvantage of the abovementioned rotating-frame solutions is the complexity, which causes a high computational burden. In order to simplify the solution, Etxeberria, et al presented a single-sequence rotating frame solution [4], which had a simple control structure and fast dynamic response, but needed the voltage positive and negative sequence extraction for the current reference calculation. On the other hand, the stationary-frame solutions are more popular due to the computational

-------------------------------------------------

saving and easy implementation. A significant contribution made by Rodriguez, et al is the flexible power control concept [5], which facilitates multiple choices for FRT (Fault Ride Through) with different current references. Other interesting methods were reported in [6-10], which achieved the flexible control of grid-connected inverters under grid faults.

However, all the abovementioned methods need a phase-locked loop (PLL). Generally speaking, a basic zero-crossing phase lock loop can be readily realized with a micro-processor unit which is also serving for realizing the controller. But for operating a grid-connected inverter under unbalanced conditions, a complicated PLL is usually required for extracting the positive and negative sequences of unbalanced grid voltages, so as to control the active and reactive powers [5-9]. That is why so many interesting and complicated PLLs have been reported in recent years，such as known DDSRF-PLL [11], DSOGI-PLL [12], CDSC-PLL [13], EPLL [14], MCCF-PLL [15] and so on [16].

Noted that these kinds of PLLs should be carefully designed [17-18]. Also, a complicated PLL in the control loop may lead to the design complexity, transient interaction and even system instability [19-20]. Therefore, using a control strategy that does not require a PLL is attractive and needs further investigation.

This paper presents an interesting control strategy for grid-connected inverter under unbalanced grid faults. It can achieve the flexible control of power and current quality without requiring a PLL.

## II. CONTROL STRATEGY

Fig.1 illustrates the schematic diagram of the grid-connected inverter. The following will present the inherent reason for the current harmonic and power oscillation of the inverter, and then provide a new flexible control structure for improving the current quality and power fluctuation without a PLL.
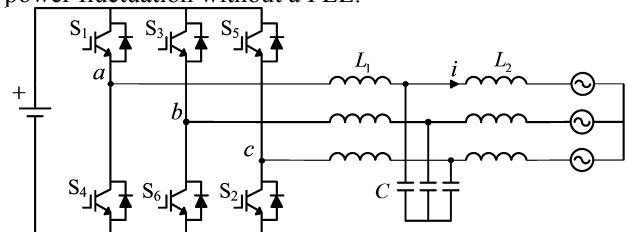


Fig. 1. Schematic diagram of grid-connected inverter

### A. Inherent reason for current harmonics

Three-phase grid voltage can be expressed as follows.

$$\begin{bmatrix} u_a \\ u_b \\ u_c \end{bmatrix} = \begin{bmatrix} U^+ \sin(\omega t + \theta_p) + U^- \sin(\omega t + \theta_n) \\ U^+ \sin(\omega t - 120° + \theta_p) + U^- \sin(\omega t + 120° + \theta_n) \\ U^+ \sin(\omega t + 120° + \theta_p) + U^- \sin(\omega t - 120° + \theta_n) \end{bmatrix} \quad (1)$$

where $U^+$, $U^-$, $\theta_p$, $\theta_n$ and $\omega$ represents the positive and negative sequence voltage amplitude, phase angle and angular frequency respectively.

With the Clarke transformation, equation (1) can be rewritten as

$$\begin{bmatrix} u_\alpha \\ u_\beta \end{bmatrix} = \frac{2}{3} \begin{bmatrix} 1 & -\frac{1}{2} & -\frac{1}{2} \\ 0 & \frac{\sqrt{3}}{2} & -\frac{\sqrt{3}}{2} \end{bmatrix} \begin{bmatrix} u_a \\ u_b \\ u_c \end{bmatrix} = \begin{bmatrix} u_\alpha^+ + u_\alpha^- \\ u_\beta^+ + u_\beta^- \end{bmatrix} \quad (2)$$

$$\begin{bmatrix} u_\alpha^+ \\ u_\beta^+ \end{bmatrix} = \begin{bmatrix} U^+ \sin(\omega t + \theta_p) \\ -U^+ \cos(\omega t + \theta_p) \end{bmatrix} \text{ and } \begin{bmatrix} u_\alpha^- \\ u_\beta^- \end{bmatrix} = \begin{bmatrix} U^- \sin(\omega t + \theta_n) \\ U^- \cos(\omega t + \theta_n) \end{bmatrix}$$

where $u_\alpha^+, u_\alpha^-, u_\beta^+, u_\beta^-$ are the positive and negative sequence components of $U_\alpha$ and $U_\beta$ in stationary frame, respectively.

According to instantaneous power theory, the active and reactive power of the inverter can be expressed as

$$\begin{bmatrix} p \\ q \end{bmatrix} = \frac{3}{2} \begin{bmatrix} u_\alpha & u_\beta \\ u_\beta & -u_\alpha \end{bmatrix} \begin{bmatrix} i_\alpha \\ i_\beta \end{bmatrix} \quad (3)$$

The grid-connected inverter output currents can be derived from (3) as

$$\begin{bmatrix} i_\alpha \\ i_\beta \end{bmatrix} = \frac{2}{3} \begin{bmatrix} u_\alpha & u_\beta \\ u_\beta & -u_\alpha \end{bmatrix}^{-1} \begin{bmatrix} P^* \\ Q^* \end{bmatrix} \quad (4)$$

where $P^*$ and $Q^*$ are the inverter output active/reactive power reference respectively.

The active and reactive current can be decomposed as

$$\begin{bmatrix} i_\alpha \\ i_\beta \end{bmatrix} = \begin{bmatrix} i_{\alpha(p)} \\ i_{\beta(p)} \end{bmatrix} + \begin{bmatrix} i_{\alpha(q)} \\ i_{\beta(q)} \end{bmatrix} = \frac{2}{3} \frac{P^*}{u_\alpha^2 + u_\beta^2} \begin{bmatrix} u_\alpha \\ u_\beta \end{bmatrix} + \frac{2}{3} \frac{Q^*}{u_\alpha^2 + u_\beta^2} \begin{bmatrix} u_\beta \\ -u_\alpha \end{bmatrix} \quad (5)$$

Substituting (2) in to (5), the current components can be obtained as follows.

$$\begin{bmatrix} i_{\alpha(p)} \\ i_{\beta(p)} \end{bmatrix} = \frac{2}{3} \frac{P^*}{\left(u_\alpha^+ + u_\alpha^-\right)^2 + \left(u_\beta^+ + u_\beta^-\right)^2} \begin{bmatrix} u_\alpha^+ + u_\alpha^- \\ u_\beta^+ + u_\beta^- \end{bmatrix} \quad (6)$$

$$\begin{bmatrix} i_{\alpha(q)} \\ i_{\beta(q)} \end{bmatrix} = \frac{2}{3} \frac{Q^*}{\left(u_\alpha^+ + u_\alpha^-\right)^2 + \left(u_\beta^+ + u_\beta^-\right)^2} \begin{bmatrix} u_\beta^+ + u_\beta^- \\ -u_\alpha^+ - u_\alpha^- \end{bmatrix} \quad (7)$$

From (6) and (7), it can be observed that the inverter current is not sinusoidal if the power reference $P^*$ and $Q^*$ are constant. The inherent reason is that the denominators of (6) and (7) are not constant, as shown in (8).

$$\left(u_\alpha^+ + u_\alpha^-\right)^2 + \left(u_\beta^+ + u_\beta^-\right)^2$$
$$= \left(U^+\right)^2 + \left(U^-\right)^2 + 2u_\alpha^+ u_\alpha^- + 2u_\beta^+ u_\beta^- \quad (8)$$
$$= \left(U^+\right)^2 + \left(U^-\right)^2 - 2U^+ U^- \cos\left(2\omega t + \theta_p + \theta_n\right)$$

The following will present a quantitative analysis of inverter current harmonics. Assuming that $\theta_p = 0$, $\theta_n = 0$, the current of $i_{\alpha(p)}$ can be expressed as

$$i_{\alpha(p)} = \frac{2}{3} \frac{P^* \left(U^+ + U^-\right)}{\left(U^+\right)^2 + \left(U^-\right)^2 - 2U^+ U^- \cos 2\omega t} \sin \omega t \quad (9)$$

With the Fourier analysis theory, $i_{\alpha(p)}$ can be expressed as

$$i_{\alpha(p)} = \frac{a_0}{2} + \sum_{n=1}^{\infty} \left(a_n \cos n\omega t + b_n \sin n\omega t\right) \quad (10)$$

where $a_0 = \frac{1}{\pi} \int_{-\pi}^{\pi} f(\omega t) d\omega t$, $a_n = \frac{1}{\pi} \int_{-\pi}^{\pi} f(\omega t) \cos n\omega t \, d\omega t$,

$$b_n = \frac{1}{\pi} \int_{-\pi}^{\pi} f(\omega t) \sin n\omega t \, d\omega t$$

With the mathematical manipulation, we can obtain that $a_n = 0$, and

$$b_n = \frac{2P^* \left(U^+ + U^-\right)}{3\pi} \int_{-\pi}^{\pi} \frac{\sin(\omega t) \sin n\omega t}{\left(U^+\right)^2 + \left(U^-\right)^2 - 2U^+ U^- \cos\left(2\omega t\right)} d\omega t \quad (11)$$

From (11), it is clear that $b_n \neq 0$ and there are many current harmonics, whose amplitudes reduce as their frequency increase. Therefore, only low-order harmonics are considered in this paper. With the system parameters listed in Table I, the total harmonic distortion (THD) of the inverter current can be calculated.

$$\text{THD}_i = \frac{\sqrt{\sum_{n=3,5,7,\cdots} (I_n)^2}}{I_1} = 31.4\% \quad (12)$$

where $I_1$ and $I_n$ are the RMS value of the fundamental and harmonic components.

Based on the above analysis, it can be observed that the inverter current will be distorted with higher THD if the inverter power is constant. Note that IEEE Std.1547 specifies that the current THD should be less than 5%. Therefore, the following will present a solution to the inverter current harmonic elimination.

### B. Current harmonic elimination and power fluctuation analysis

As discussed in the previous section, the inherent reason for the inverter current harmonics comes from $2U^+ U^- \cos(2\omega t)$ in (11). Therefore, the current harmonics can be eliminated on condition that $2U^+ U^- \cos(2\omega t)$ is cancelled, which can be easily achieved with a notch filter of $F(s)$. Then (6) and (7) can be rewritten as

$$\begin{bmatrix} i_{\alpha(p)} \\ i_{\beta(p)} \end{bmatrix} = \frac{2}{3} \frac{P^*}{[\left(u_\alpha^+ + u_\alpha^-\right)^2 + \left(u_\beta^+ + u_\beta^-\right)^2] F(s)} \begin{bmatrix} u_\alpha^+ + u_\alpha^- \\ u_\beta^+ + u_\beta^- \end{bmatrix}$$
$$= \frac{2}{3} \frac{P^*}{\left(U^+\right)^2 + \left(U^-\right)^2} \begin{bmatrix} u_\alpha^+ + u_\alpha^- \\ u_\beta^+ + u_\beta^- \end{bmatrix} \quad (13)$$

$$\begin{bmatrix} i_{\alpha(q)} \\ i_{\beta(q)} \end{bmatrix} = \frac{2}{3} \frac{Q^*}{[\left(u_\alpha^+ + u_\alpha^-\right)^2 + \left(u_\beta^+ + u_\beta^-\right)^2] F(s)} \begin{bmatrix} u_\beta^+ + u_\beta^- \\ -u_\alpha^+ - u_\alpha^- \end{bmatrix}$$
$$= \frac{2}{3} \frac{Q^*}{\left(U^+\right)^2 + \left(U^-\right)^2} \begin{bmatrix} u_\beta^+ + u_\beta^- \\ -u_\alpha^+ - u_\alpha^- \end{bmatrix} \quad (14)$$

It should be noted that the notch filter $F(s)$ here is a key piece of the control strategy. Therefore, its role and structure design should be discussed. Since the role of the notch filter $F(s)$ is to cancel the term of $2U^+ U^- \cos(2\omega t)$ in (11), its structure is designed as

$$F(s) = \frac{s^2 + \omega_n^2}{s^2 + \xi\omega_n s + \omega_n^2} \qquad (15)$$

where $\omega_n$ $\omega_n$ is the notch frequency which is the same as that of $2U^+U^-\cos(2\omega t)$ in (11), and $\xi\omega_n$ is the cutoff frequency of the notch filter. In this paper, $\xi$ is set to 1 for the good dynamic response as well as the filter performance.

In this way, the inverter current only consists of the fundamental positive and negative components, excluding the harmonic components. However, the power fluctuation will appear in this case, and the active and reactive power fluctuations can be expressed as follows.

$$\tilde{p} = \frac{3}{2}\left(u_\alpha^- u_\alpha^+ + u_\beta^- u_\beta^+ + u_\alpha^+ u_\alpha^- + u_\beta^+ u_\beta^-\right) \qquad (16)$$

$$\tilde{q} = \frac{3}{2}\left(u_\beta^+ u_\alpha^- - u_\alpha^+ u_\beta^- - u_\alpha^- u_\beta^+ + u_\beta^- u_\alpha^+\right) \qquad (17)$$

Equation (13) and (14) can be rewritten as

$$i_\alpha^+ = \frac{2}{3}\frac{u_\alpha^+ P^*}{\left(U^+\right)^2 + \left(U^-\right)^2} + \frac{2}{3}\frac{u_\beta^+ Q^*}{\left(U^+\right)^2 + \left(U^-\right)^2} \qquad (18)$$

$$i_\beta^+ = \frac{2}{3}\frac{u_\beta^+ P^*}{\left(U^+\right)^2 + \left(U^-\right)^2} + \frac{2}{3}\frac{-u_\alpha^+ Q^*}{\left(U^+\right)^2 + \left(U^-\right)^2} \qquad (19)$$

$$i_\alpha^- = \frac{2}{3}\frac{u_\alpha^- P^*}{\left(U^+\right)^2 + \left(U^-\right)^2} + \frac{2}{3}\frac{u_\beta^- Q^*}{\left(U^+\right)^2 + \left(U^-\right)^2} \qquad (20)$$

$$i_\beta^- = \frac{2}{3}\frac{u_\beta^- P^*}{\left(U^+\right)^2 + \left(U^-\right)^2} + \frac{2}{3}\frac{-u_\alpha^- Q^*}{\left(U^+\right)^2 + \left(U^-\right)^2} \qquad (21)$$

Substituting (18)~(21) and (2) into (16) and (17), the power fluctuations can be obtained as follows.

$$\begin{aligned}\tilde{p} &= \frac{2P^*}{\left(U^+\right)^2 + \left(U^-\right)^2}\left(u_\alpha^+ u_\alpha^- + u_\beta^+ u_\beta^-\right) \\ &= \frac{-2P^*U^+U^-}{\left(U^+\right)^2 + \left(U^-\right)^2}\cos\left(2\omega t + \theta_p + \theta_n\right)\end{aligned} \qquad (22)$$

$$\begin{aligned}\tilde{q} &= \frac{2Q^*}{\left(U^+\right)^2 + \left(U^-\right)^2}\left(u_\alpha^- u_\alpha^+ + u_\beta^+ u_\beta^-\right) \\ &= \frac{-2Q^*U^+U^-}{\left(U^+\right)^2 + \left(U^-\right)^2}\cos\left(2\omega t + \theta_p + \theta_n\right)\end{aligned} \qquad (23)$$

With the system parameters listed in Table I, the active and reactive power fluctuations can be obtained as $\tilde{p} = -138.27\cos 2\omega t$, $\tilde{q} = -110.6\cos 2\omega t$, and the peak-peak values are 276.54 W and 221.2 Var, respectively.

### C. Flexible control of current harmonics and power fluctuations

In order to achieve the flexible control of current harmonics and power fluctuations, a new solution is proposed by combing both abovementioned methods with an adjustable coefficient as follows.

$$i_{\alpha p}^* = \frac{2}{3}P^*\left\{\frac{ku_\alpha}{\left(u_\alpha\right)^2 + \left(u_\beta\right)^2} + \frac{(1-k)u_\alpha}{[\left(u_\alpha\right)^2 + \left(u_\beta\right)^2]F(s)}\right\} \qquad (24)$$

$$i_{\beta p}^* = \frac{2}{3}P^*\left\{\frac{ku_\beta}{\left(u_\alpha\right)^2 + \left(u_\beta\right)^2} + \frac{(1-k)u_\beta}{[\left(u_\alpha\right)^2 + \left(u_\beta\right)^2]F(s)}\right\} \qquad (25)$$

$$i_{\alpha q}^* = \frac{2}{3}Q^*\left\{\frac{ku_\beta}{\left(u_\alpha\right)^2 + \left(u_\beta\right)^2} + \frac{(1-k)u_\beta}{[\left(u_\alpha\right)^2 + \left(u_\beta\right)^2]F(s)}\right\} \qquad (26)$$

$$i_{\beta q}^* = \frac{2}{3}Q^*\left\{\frac{-ku_\alpha}{\left(u_\alpha\right)^2 + \left(u_\beta\right)^2} + \frac{-(1-k)u_\alpha}{[\left(u_\alpha\right)^2 + \left(u_\beta\right)^2]F(s)}\right\} \qquad (27)$$

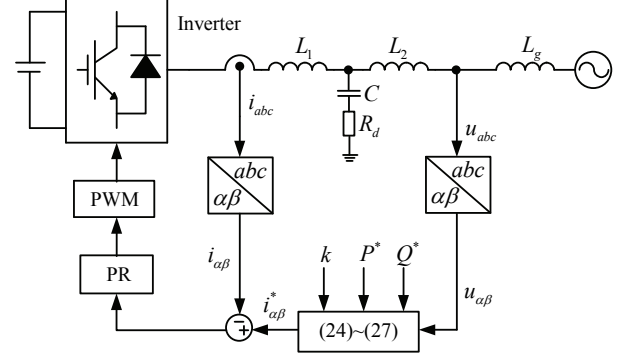where $k$ represents the adjustable coefficient, and $0 \le k \le 1$.



Fig. 2. Single-line diagram of system control structure

The control structure of the proposed method is shown in Fig. 2, where $L_g$ is used to emulate the impedance of weak grid. $R_d$ is used to damping the potential resonance from LCL filter and grid impedance, and optimization of the damping resistor can be found in [21], which is beyond the scope of this paper. Considering that the current harmonic amplitude reduces as its frequency increases, only low-order current harmonics are regulated with PR controller [22]. Note that, for operating PR controller under grid frequency variation, its resonant frequency should be updated with the grid frequency, which can be easily estimated in a fast and accurate way as reported in [23]. Under weak grid, especially under unbalanced weak grid, it is very complex to carry out the control parameter design and stability analysis. The main reason is that only the positive sequence model is considered under balanced grid. But for the unbalanced weak grid, not only positive sequence model, but also negative sequence model, as well as the weak grid impedance all should be considered. The systematic and comprehensive modeling and stability analysis under weak and unbalanced conditions would be a subject of our future research.

It should be noted that the proposed control structure in Fig. 2 is single-current-loop solution. It would be interesting whether P-Q regulator could be used. In this case, another power loop with PI control should be integrated with the existing current loop. It might be beneficial for the power regulation, but lead to the control complicity due to two-loop (power-current-loop) structure with two PI coefficients tuning to avoid interaction between outer power loop and inner current loops. That's why the current-loop structure is used for most existing solutions. On the other hand, for high penetration of grid-connected inverters, P-Q regulator with droop control might be an interesting solution for multi-inverter microgrid applications under unbalanced conditions.

## III. Experimental Results

In order to verify the effectiveness of the proposed method, the experimental tests are carried out. A DC Power source (Chroma 62050H-600) is used to emulate the renewable energy sources and storage. A Programmable AC source (Chroma 6590) is used to emulate the grid fault. The inverter is controlled by a 32-bit fixed-point 150MHz TMS320F2812 DSP. The switching and control frequency are set to 10 kHz. The system parameters are listed as follows.

TABLE I.    System Parameters

| Parameters | Value | Parameters | Value |
|---|---|---|---|
| DC bus/V | 120 | $u_a$/V | $50\angle 0°$ |
| $u_b$/V | $34.2\angle -137°$ | $u_c$/V | $34.2\angle 137°$ |
| P*/ W | 250 | Q*/ Var | 200 |
| $L_1$/mH | 5 | $L_2$/mH | 1 |
| C/μF | 9.9 | 0.0~0.2s | $k = 0$ |
| 0.2~0.4s | $0<k<1$ | 0.4~0.6s | $k = 1$ |

Fig. 3 ~ Fig. 5 shows the experimental results under stiff grid, where the grid impedance $L_g$=0. Fig. 3 shows the experimental results with $k$=1. It can be observed that the inverter currents are distorted with larger low-order harmonics, which is consistent with the above theoretical analysis. On the other hand, the active and reactive power of the inverter is almost constant. In order to verify the system dynamic response, a step change of the reactive power reference from 0 Var to 200 Var occurred at 0.03s. As can be seen, the system transient response is very fast due to the controller not requiring a PLL for the positive and negative sequence separation.

Fig. 4 shows the experimental results with $k$=0. It can be observed that the current harmonics are significantly reduced, while the power fluctuations increase, the peak-peak values of the active and reactive power fluctuation are about 280 W and 220 Var, which is in agreement with the theoretical analysis.
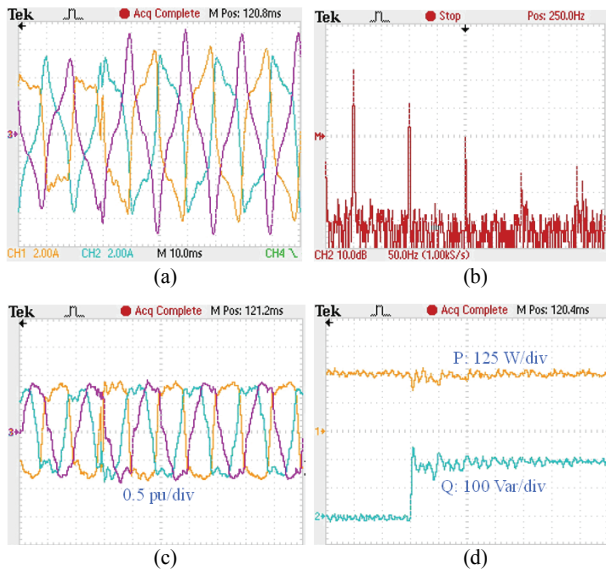


Fig. 3.  Experimental results of constant power control. (a) grid current (b) current harmonic spectrum, (c) modulation waveform, (d) inverter power
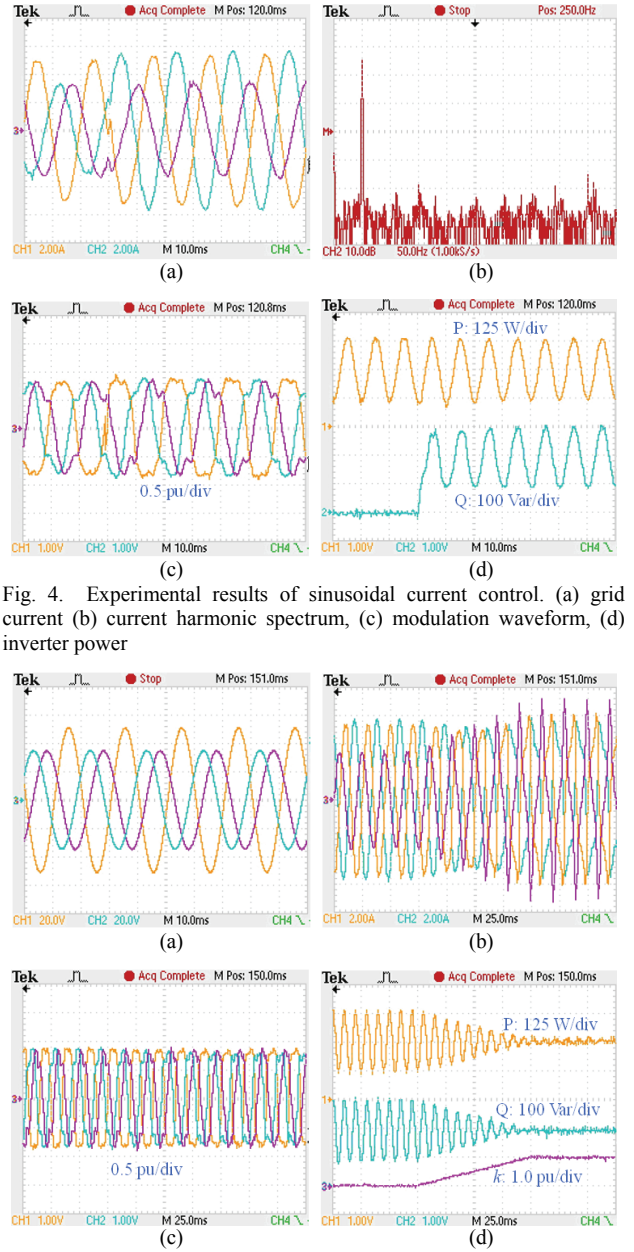


Fig. 4.  Experimental results of sinusoidal current control. (a) grid current (b) current harmonic spectrum, (c) modulation waveform, (d) inverter power



Fig. 5.  Experimental results of proposed method under unbalanced conditions. (a) grid voltage, (b) grid current, (c) inverter modulation waveform, (d) inverter output power

Fig. 5 shows the experimental results of the proposed control structure with an increasing value of $k$. It can be observed that the current harmonics increase and power fluctuations reduce as the coefficient of $k$ rises. It should be noted that the inverter peak current is affected by the adjustment coefficient of $k$. An interesting observation is that the inverter current amplitude approaches the minimum value when $k$=0.5, while the amplitude reaches its maximum value when $k$=1. Therefore, the following factors should be considered for selecting the coefficient $k$ to make a tradeoff among the current harmonics, power fluctuations, as well as the peak current. In general, when the coefficient $k$ is small, the current waveform is better but the power oscillation is large, whereas the current harmonic is increased with larger $k$. In good agreement with the Instantaneous Power Theory, we can not achieve both good current waveform and constant power oscillation under unbalanced conditions. Therefore, selecting the coefficient $k$ highly depends on the specific

applications. In practice, the peak current is one of the most important factors to ensure the safe operation of inverter to avoid overcurrent [24]. From this viewpoint, it would be better that $k$=0.5, where the peak current is minimized with a tradeoff of current harmonics and power oscillations. On the other hand, for the applications sensitive to power oscillations or current harmonics, $k$ should be selected around 1 or 0 respectively.

In order to verify the effectiveness of the proposed method under weak grid conditions, an inductor $L_g$ is inserted as shown in Fig. 2. There are various definitions of a weak grid [25-26]. In this paper, the grid impedance is 2.5 mH. It should be noted that this paper mainly focuses on the grid connected inverter in low voltage grid. For the high voltage power system, the weak grid condition will be more complex, which would be the subject of our future research.
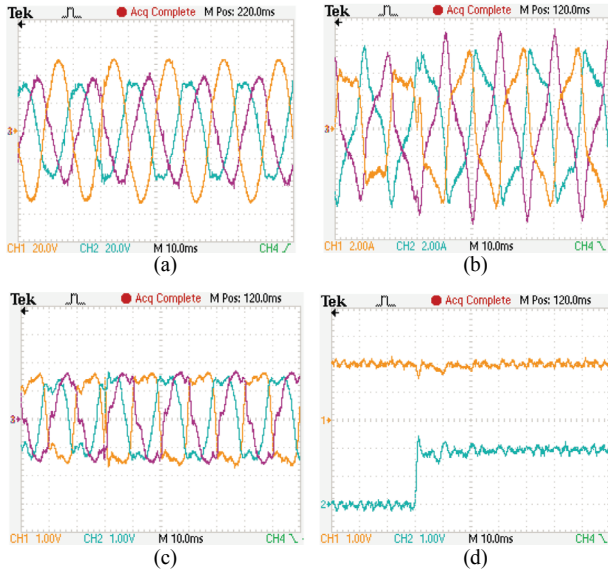


Fig. 6. Experimental results of proposed method under weak grid with $k$=1. (a) PCC voltage, (b) grid current, (c) inverter modulation waveform, (d) inverter output power



Fig. 7. Experimental results of proposed method under weak grid with $k$=0. (a) PCC voltage, (b) grid current, (c) inverter modulation waveform, (d) inverter output power
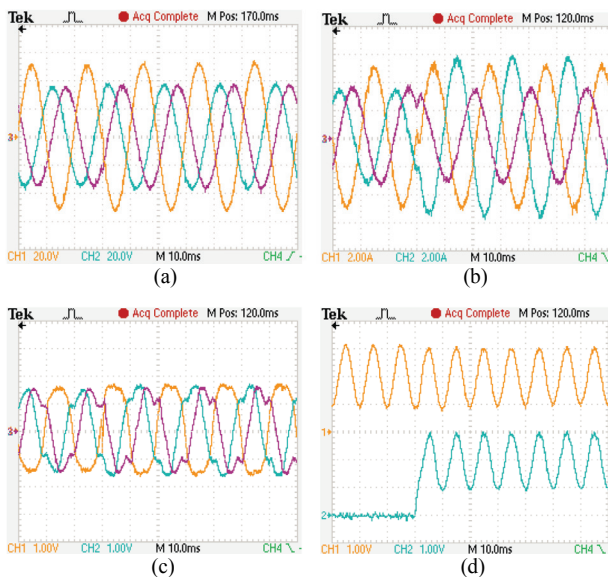


Fig. 8. Experimental results of proposed method under weak grid with 0<$k$<1. (a) PCC voltage, (b) grid current, (c) inverter modulation waveform, (d) inverter output power
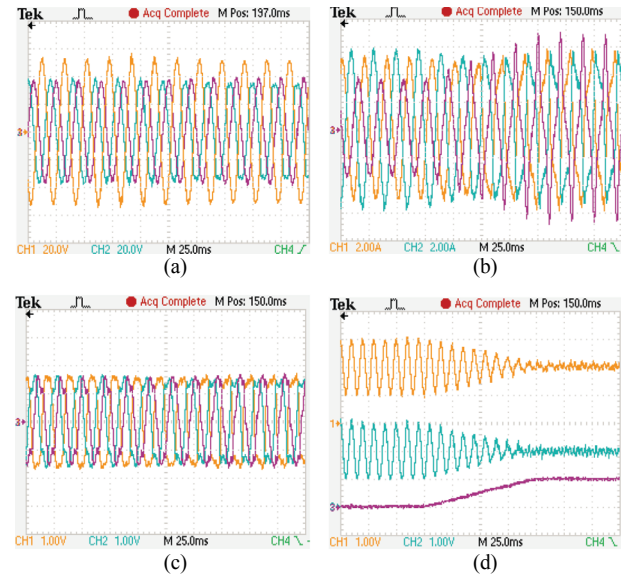
Fig. 6 ~ Fig. 8 shows the experimental results under weak grid, where the grid impedance $L_g$ = 2.5mH. It can be observed that the experimental results are similar to those under stiff grid, except that PCC voltage is slight distorted by the inverter current harmonic, as shown in Fig. 6(a). In summary, the proposed solution works well under both stiff and weak grid conditions.

## IV. CONCLUSION

This paper has presented a new control structure for the grid-connected inverter. In contrast with the existing methods, the proposed method can achieve the flexible control of power and current quality without requiring a PLL. The experimental results demonstrate that the proposed method is effective and has a fast dynamic response. Therefore, it is attractive for flexible operation of grid-connected inverter under unbalanced grid faults.

## REFERENCES

[1]  H.-S. Song and K. Nam, "Dual current control scheme for PWM converter under unbalanced input voltage conditions," *IEEE Trans. Ind. Electron.*, vol. 46, no. 5, pp. 953–959, Oct. 1999.
[2]  M. Reyes, P. Rodriguez, S. Vazquez, A. Luna, R. Teodorescu, and J. M. Carrasco, "Enhanced decoupled double synchronous reference frame current controller for unbalanced grid-voltage conditions," *IEEE Trans. Power Electron.*, vol. 27, no. 9, pp. 3934–3943, Sep. 2012.
[3]  P. Xiao, K. A. Corzine, and G. K. Venayagamoorthy, "Multiple reference frame-based control of three-phase PWM boost rectifiers under unbalanced and distorted input conditions," *IEEE Trans. Power Electron.*, vol. 23, no. 4, pp. 2006–2017, Jul. 2008.
[4]  I. Etxeberria-Otadui, U. Viscarret, M. Caballero, A. Rufer, and S. Bacha, "New optimized PWM VSC control structures and strategies under unbalanced voltage transients," *IEEE Trans. Ind. Electron.*, vol. 54, no. 5, pp. 2902–2914, Oct. 2007.
[5]  P. Rodriguez, A. Timbus, R. Teodorescu, M. Liserre, and F. Blaabjerg, "Flexible active power control of distributed power generation systems during grid faults," *IEEE Trans. Ind. Electron.*, vol. 54, no. 5, pp. 2583–2592, Oct. 2007.
[6]  M. Castilla, J. Miret, J. L. Sosa, J. Matas, and L. G. Vicuna, "Grid fault control scheme for three-phase photovoltaic inverters with adjustable power quality characteristics," *IEEE Trans. Power Electron.*, vol. 25, no. 12, pp. 2930–2940, Dec. 2010.
[7]  A. Junyent-Ferre, O. Gomis-Bellmunt, T.C. Green, and D.E. Soto-Sanchez, "Current control reference calculation issues for the operation of renewable source grid interface VSCs under

unbalanced voltage sags," *IEEE Trans. Power Electron.*, vol. 26, no. 12, pp. 3744–3753, Dec. 2011.

[8]  F. Wang, J. L. Duarte, and M. A. M. Hendrix, "Pliant active and reactive power control for grid-interactive converters under unbalanced voltage dips," *IEEE Trans. Power Electron.*, vol. 26, no. 5, pp. 1511–1521, May 2011.

[9]  Z. R. Ivanovic, E. M.Adžić, M. S. Vekić, S. U. Grabić, N. L. Čelanović, and V. A. Katić, "HIL evaluation of power flow control strategies for energy storage connected to smart grid under unbalanced conditions," *IEEE Trans. Power Electron.*, vol. 27, no. 11, pp. 4699–4710, Nov. 2012.

[10] X. Guo, X, Zhang, B. Wang, W. Wu, and J. M. Guerrero, "Asymmetrical grid fault ride-through strategy of three-phase grid-connected inverter considering network impedance impact in low-voltage grid," *IEEE Trans. Power Electron.*, vol. 29, no. 3, pp. 1064–1068, Mar. 2014.

[11] P. Rodriguez, J. Pou, J. Bergas, J. Candela, R. Burgos, and D. Boroyevich, "Decoupled double synchronous reference frame PLL for power converters control," *IEEE Trans. Power Electron.*, vol. 22, no. 2, pp. 584–592, Mar. 2007.

[12] P. Rodriguez, A. Luna, I. Etxeberria, R. Teodorescu, and F. Blaabjerg, "A stationary reference frame grid synchronization system for three-phase grid-connected power converters under adverse grid conditions," *IEEE Trans. Power Electron.*, vol. 27, no. 1, pp. 99–112, Jan. 2012.

[13] Y. F. Wang, and Y. W. Li, "Analysis and digital implementation of cascaded delayed-signal-cancellation PLL," *IEEE Trans. Power Electron.*, vol. 26, no. 4, pp. 1067-1080, Apr. 2011.

[14] M. Karimi-Ghartemani and M. Iravani, "A method for synchronization of power electronic converters in polluted and variable-frequency environments," *IEEE Trans. Power Syst.*, vol. 19, no. 3, pp. 1263–1270, Aug. 2004

[15] X. Guo, W. Wu, and Z. Chen, "Multiple-complex coefficient-filter-based phase-locked loop and synchronization technique for three-phase grid interfaced converters in distributed utility networks," *IEEE Trans. Ind. Electron.*, vol. 58, no. 4, pp. 1194–1204, Apr. 2011.

[16] I. Carugati, S. Maestri, P. G. Donato, D. Carrica, and M. Benedetti, "Variable sampling period filter PLL for distorted three-phase systems," *IEEE Trans. Power Electron.*, vol. 27, no. 1, pp. 321–330, Jan. 2012.

[17] S. Golestan, M. Ramezani, J. M. Guerrero, F. D. Freijedo, and M. Monfared, "Moving average filter based phase-locked loops: performance analysis and design guidelines," *IEEE Trans. Power Electron.*, vol. 29, no. 6, pp. 2750-2763, Jun. 2014

[18] S. Golestan, M. Monfared, and F. D. Freijedo, "Design-oriented study of advanced synchronous reference frame phase-locked loops," *IEEE Trans.Power Electron.*, vol. 28, no. 2, pp. 765–778, Feb. 2013.

[19] M. Cespedes and J. Sun, "Impedance modeling and analysis of grid connected voltage-source converters," *IEEE Trans. Power Electron.*, vol. 29, no. 3, pp. 1254–1261, Mar. 2014.

[20] M. Cespedes and J. Sun, "Adaptive control of grid-connected inverters based on online grid impedance measurements," *IEEE Trans. Sustain. Energy*, vol. 5, no. 2, pp. 516–523, Apr. 2014.

[21] R. Pena-Alzola, M. Liserre, F. Blaabjerg, R. Sebastian, J. Dannehl, and F. W. Fuchs, "Analysis of the passive damping losses in LCL-filter-based grid converters," *IEEE Trans. Power Electron.*, vol. 28, no. 6, pp. 2642– 2646, Jun. 2013.

[22] A. Vidal, F. D. Freijedo, A. G. Yepes, P. Fernandez-Comesana, J. Malvar, O. Lopez, and J.Doval-Gandoy, "Assessment and optimization of the transient response of proportional-resonant current controllers for distributed power generation systems," *IEEE Trans. Ind. Electron.*, vol. 60, no. 4, pp. 1367–1383, Apr. 2013.

[23] K.-J. Lee, J.-P. Lee, D. Shin, D.-W. Yoo, and H.-J. Kim, "A novel grid synchronization PLL method based on adaptive low-pass notch filter for grid-connected PCS," *IEEE Trans. Ind. Electron.*, vol. 61, no. 1, pp. 292– 301, Jan. 2014.

[24] J. Miret, M. Castilla, A. Camacho, L. G. Vicuna, and J. Matas, "Control scheme for photovoltaic three-phase inverters to minimize peak currents during unbalanced grid-voltage sags," *IEEE Trans. Power Electron.*, vol. 27, no. 10, pp. 4262–4271, Oct. 2012

[25] I. J. Gabe, V. F. Montagner, and H. Pinheiro, "Design and implementation of a robust current controller for VSI connected to the grid through an LCL filter," *IEEE Trans. Power Electron.*, vol. 24, no. 6, pp. 1444–1452, Jun. 2009.

[26] S. Yang, Q. Lei, F. Z. Peng, and Z. Qian, "A robust control scheme for grid-connected voltage-source inverters," *IEEE Trans. Ind. Electron.*, vol. 58, no. 1, pp. 202–212, Jan. 2011.